Talanta Open 11 (2025) 100437

Contents lists available at ScienceDirect

Talanta Open

journal homepage: www.sciencedirect.com/journal/talanta-open

Argon versus helium as carrier gas for LA-ICP-MS impurity mapping on ice cores

Pascal Bohleber [a,b,*], Kristina Mervič [c], Remi Dallmayr [a], Ciprian Stremtan [d], Martin Šala [e]

[a] Alfred Wegener Institute Helmholtz Centre for Polar and Marine Research, Bremerhaven, Germany
[b] Department of Geosciences, Goethe University Frankfurt, Frankfurt, Germany
[c] Department of Catalysis and Chemical Reaction Engineering, National Institute of Chemistry, Ljubljana, Slovenia
[d] Teledyne Photon Machines, Bozeman, MT, USA
[e] Department of Analytical Chemistry, National Institute of Chemistry, Ljubljana, Slovenia

ARTICLE INFO

Keywords:
Ice core impurity analysis
LA-ICP-MS
Mapping
Carrier gas

ABSTRACT

Impurity records in polar ice cores have provided invaluable insights into atmospheric aerosol concentrations of the past environment. The investigation of the oldest, deepest and highly thinned ice core layers is one of the most pressing tasks in today's state-of-the-art ice core research. This calls for impurity analysis at high spatial resolution, which has to take into account post-depositional processes through the interaction of impurities with the ice matrix. To this end, mapping the impurity distribution in ice with laser ablation inductively-coupled plasma mass spectrometry (LA-ICP-MS) has great potential. Here we explore to what extent the use of Ar as a carrier gas has merits in ice core impurity mapping with LA-ICP-MS. This is motivated by the fact that a) the use of Ar is more economical over He, especially when used in conjunction with large volume sample cells, and b) an increase in sensitivity has previously been reported when adding "wet" Ar to He as a carrier gas. We show that, albeit not fully matching the single-pulse-performance of He, it is possible to achieve mapping at up to 500 Hz with Ar in a system that is originally designed for He. In contrast to what we find on NIST glass standards and a sample of decorative murrina glass, maps obtained on ice core samples show higher intensities in Ar than in He. In an extreme case example, we show how Ar may permit to obtain signals in a deep interglacial ice sample from Antarctica with very low impurity concentrations, which was not possible when using He with the same LA-ICP-MS system.

1. Introduction

Polar ice cores are a unique archive of past climate variability, with aerosol-related atmospheric impurities trapped in the ice delivering an important set of climate proxies [e.g. 1,2]. Understanding to what degree impurities in the deepest and highly thinned ice core layers preserve their original message still marks a frontier in ice core research [3–5]. Breaking this frontier becomes more pressing than ever as new efforts are underway to retrieve climatic records older than 1 million years from Antarctica stored in the deepest ice at some locations [6,7]. Due to the sub-mm depth resolution required to succeed, this task goes beyond the current state-of-the-art of analytical techniques. The intricate interplay of impurities with the ice matrix cannot be fully explored when analyzing meltwater, hence techniques analyzing ice cores in their solid state are indispensable [8]. Ice core impurity analysis using laser ablation inductively-coupled plasma mass spectrometry (LA-ICP-MS) has unique potential in this context due to its micron-resolution and micro-destructiveness [9,10]. Since its early phase in ice core analysis this technique has been employed to investigate the localization of impurities within the ice [11,12]. Recent adaptions for two-dimensional high-resolution impurity mapping of ice cores are now fully capitalizing on this approach at resolutions of tens of microns, providing unprecedented detail about the impurity localization within the ice matrix [13]. Mostly water-soluble species such as Na are found primarily at grain boundaries, with mostly signal-free grain interiors [14]. The technique is currently further evolving to cover a broad spectrum of elements, especially when coupling a laser ablation system with a cryogenic sample holder to a "time-of-flight" mass spectrometer (cryo-LA-ICP-TOFMS) [15]. To fully succeed in utilizing the full potential of LA-ICP-MS for the analysis of the "Oldest Ice" from Antarctica,

* Corresponding author.
E-mail address: pascal.bohleber@awi.de (P. Bohleber).

https://doi.org/10.1016/j.talo.2025.100437
Received 20 January 2025; Received in revised form 14 March 2025; Accepted 17 March 2025
Available online 21 March 2025

several important challenges still lie ahead. First, sensitivity is a key issue because Antarctic ice constitutes a highly pure matrix, with most elemental impurities in the low µg/L or "parts per billion" (ppb) concentration range or even lower – if analyzed as meltwater. Recent approaches at quantitative mapping using LA-ICP-MS revealed that, although the high degree of spatial localization within the ice amplifies the concentration, Antarctic interglacial ice may have only a few tens of ppb of Na at the grain boundaries and most other elemental analytes are at or below the limit of detection (LOD) [16]. Second, processing more than 100 m of ice core depth from the deep sections of an "Oldest Ice Core" will require high throughput analysis without sacrificing analytical performance. This can be achieved through large cryocell technology capable of 2D mapping [8]. However, the comparatively large internal volume of such cells also increases the consumption of He used as a carrier gas and thus the cost of consumables. Other existing large cryocells for 1D analysis use Ar as a carrier gas [10,17], based on the pioneering work by Reinhardt et al. [18] who also employed Ar as a carrier gas. The use of He versus other carrier gases, primarily Ar and N_2, has been widely explored from an analytical point of view and with regard to aerosol formation and transport [e.g. [19–21]]. Of special importance for ice analysis - which inherently involves ablation of a water-based matrix, an increase in sensitivity has been reported for mixtures between He and "wet" Ar due to increased vaporization efficiency in the ICP [22,23]. With this background we explore here the use of Ar as an alternative carrier gas to He, with special focus on mapping the impurity distribution in ice cores. We use decorative murrina glass as a non-cryogenic model system to evaluate the mapping performance and compare mapping under He versus Ar conditions in deep Antarctic interglacial ice with low impurity concentrations.

2. Materials and methods

2.1. LA-ICP-MS ice core analysis at AWI

The newly established cryo-LA-ICP-TOFMS system at the Alfred Wegener Institute Helmholtz Centre for Polar and Marine Research, Bremerhaven (AWI) comprises a 193 nm excimer laser ablation system capable of repetition rates up to 1 kHz (Iridia by Teledyne Photon Machines, Bozeman, MT, USA) coupled to a "time-of-flight" ICP-MS (Vitesse ICP-TOF-MS by Nu Instruments, Wrexham, UK) (Fig. 1). The laser ablation system is equipped with a cryogenic sample cell (Cryo-COBALT Cell, Teledyne Photon Machines), in which a Nickel-coated copper baseplate is cooled down using water-cooled Peltier elements. In contact with the actively cooled baseplate, stainless steel sample trays transfer the cooling to the ice samples from three sides. The temperature is regulated via an integrated PID algorithm, allowing to maintain the surface temperature of the samples below − 20°C with a stability higher than ±1°C over more than 8 h. The aerosol collection is achieved by two different modules, which can be interchanged: a "cup cell" configuration and a "tube cell" configuration, the latter primarily designed for smaller spots and very fast single pulse response (SPR) in the range of single digits ms. Both configurations allow to adjust the distance between the cell and the sample surface using a motorized a dedicated z'-stage, independent of the primary z-stage [24,25]. We tested both configurations using specific carrier gas flow conditions for both He and Ar.

An ARIS (Aerosol Rapid Introduction System, Teledyne Photon Machines) is used for fast aerosol transfer to the ICP-TOFMS [24]. Using a NIST SRM 612 synthetic glass standard as a certified reference material, instrumental parameters are optimized for best sensitivity in the mass range up to m/z=90 (comprising the mass range of primarily interesting analytes for ice) and minimum oxides. For ice samples, only the narrowed mass ranges from m/z=23 up to m/z=90 was acquired. We used NIST SRM 612 to tune the system (gas flow in the sample chamber, distance between cell and sample surface) in order to optimize the SPR (gas conditions and tuned SPR indicated in Table 1). The entire setup is operated within a clean laboratory at AWI.

Following a previously established best-practice approach, the ice surface was decontaminated by scraping with a major-element free ceramic ZrO_2 blade (American Cutting Edge, USA) immediately before inserting the samples into the ablation chamber. Prior to obtaining maps on the ice, the respective location was also cleaned by pre-ablation (fluence 2 J cm^{-2}, 40 µm beam size, dosage 5). All maps on ice were obtained using a 10 µm circular spot, fluence 4 J cm^{-2} and dosage 10 (10 overlapping spots per pixel) if not noted otherwise. The final maps were compiled using the HDIP software (Teledyne Photon Machines).

Analyzed ice samples were obtained from the EPICA Dome C (EDC) ice core drilled in central Antarctica [26]. EDC1819-3 (ca. 1000 m depth) and EDC5600-6 (ca. 3080 m depth) represent ice conditions from a comparatively impurity-rich glacial and a deep interglacial period with low impurity concentrations, respectively. As a model system for testing mapping performance, we also used a piece of decorative murrina glass, embedded in epoxy resin and polished, following a previously employed approach [27].

Table 1
Instrumental parameters used at the AWI LA-ICP-MS system, including carrier gas parameters used in Cup and Tube cell configuration for He and Ar, respectively.

LA (Iridia 1 kHz, ARIS)		ICP-MS (Vitesse)		
Wavelength (nm)	193	RF power (W)	1300	
Fluence (J cm^{-2})	4	Auxiliary gas flow (L min^{-1})	2	
Repetition rate	250 / 500	Coolant flow (L min^{-1})	13	
Dosage	10	Nebulizer flow (L min^{-1})	1.25	
Beam size (µm)	10	Reaction cell gas (mL min^{-1})	7 (He) / 12 (H_2)	
Carrier gas parameters	**Cup cell**		**Tube cell**	
	He	Ar	He	Ar
Carrier gas flow (L min^{-1})	0.3	0.3	0.13-0.15	0.09-0.11
Single pulse response (ms)	5	>100	4	20–50

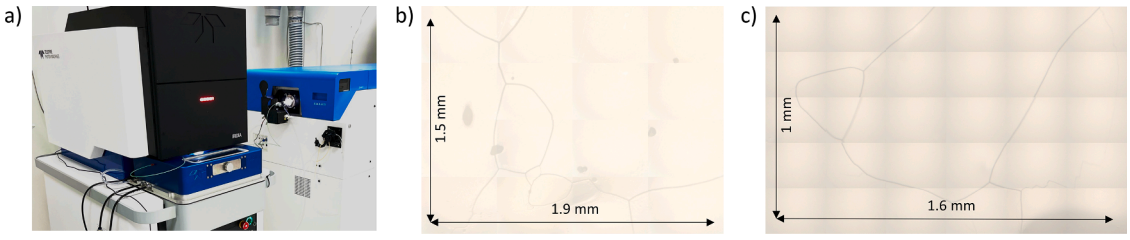

Fig. 1. The LA-ICP-TOFMS setup at AWI equipped with a cryogenic sample holder and rapid aerosol transfer line (a). The cryoholder keeps the ice sample surface temperature stable below − 20°C. Ice samples stay frozen without any visual indication for microscopic melting at the surface. Parts b) and c) show two optical mosaic images of the ice sample surfaces analyzed here (see text). Individual ice grains can be clearly distinguished by their boundaries (dark lines).

2.2. LA-ICP-MS ice core analysis at NIC

The LA-ICP-MS experiments were conducted at the National Institute of Chemistry, Ljubljana (NIC), using an Analyte G2 193 nm ArF* excimer laser ablation system (Teledyne Photon Machines) equipped with a HelEx II standard two-volume ablation cell. The system was coupled to an Agilent 7900x quadrupole ICP-MS instrument (Agilent Technologies, Santa Clara, CA, USA) via the Aerosol Rapid Introduction System (ARIS) from Teledyne Photon Machines. Line scans were performed on NIST SRM 610 and 612 glass standards to investigate the signal intensity and signal-to-noise ratio (SNR) for Li, Y, Th, and U under varying carrier gas conditions. The tests included 100 % He, 100 % Ar, and He/Ar mixtures with 25 %, 50 %, and 75 % Ar as a carrier gas, using three beam sizes (10 μm, 20 μm, and 35 μm). Operational parameters for these experiments are summarized in Table 2.

To further examine the effects of carrier gas composition, additional tests were conducted using a cryo cell under both warm and cold conditions. For this, the NIC LA-ICP-MS system was temporarily modified with a cryostage and portable chiller developed for the LA-ICP-MS system at Ca'Foscari University of Venice [13], enabling sample cooling to temperatures below − 20 °C. Experiments with 100 % He and 100 % Ar as carrier gases were repeated in the cryo cell to assess their influence on signal intensity, SNR, and ablation performance for the same elements. Following the LA-ICP-MS analyses, the morphology of the ablation craters was examined to evaluate ablation efficiency and differences in crater shapes, depths, and volumes under each experimental condition. The surface topography of the NIST SRM 610 and 612 standards and the murrina surface was analyzed using an optical interferometer (Zegage PRO HR, Zygo Corporation, Middlefield, CT, USA). Measurements were performed with a 50 × magnification lens, achieving a lateral resolution of 0.173 μm and a surface topography repeatability of less than 3.5 nm. The 3D surface data were processed using the manufacturer's Mx™ software (version 8.0.0.23), and the "sur" and "int" files were imported into MATLAB R2020a (MathWorks) for conversion to CSV format. Missing data, attributed to steeply sloped areas, were interpolated using MATLAB's regionfill function.

3. Results

3.1. Crater volume and signal intensity on NIST glass standards

Using the profilometer at NIC analogue to previous work [28], crater volumes were evaluated for 10, 20 and 35 μm square spots. Fig. 2 shows the results for pure He and Ar condition as well as various mixes, as well as pure Ar conditions using the cryogenic holder with and without cooling turned on ("cryo cold" vs "cryo warm"). Fig. 3 shows the respective crater morphology.

Both on NIST SRM 612 and NIST SRM 610 glass standards, we find no change in the ablated volume with increasing percentage of Ar in the carrier gas. The cooling in the cryogenic holder also has no significant effect on the crater volume with respect to the same conditions without cooling. Running an array of line profiles on NIST SRM 610 and 612, the corresponding intensities show a clear decrease at 100 % Ar with respect to 100 % He (Fig. 4). For low masses (^{7}Li, ^{89}Y) the intensity decreases with increasing percentage of Ar, while for ^{238}U, there is tentative evidence for a minor increase in sensitivity up to 50 % Ar/He. It has to be noted that the signal stability decreases with increasing percentage of Ar in the carrier gas. While the relative standard deviations (RSD) remain below 5 % with 100 % He, they increase to 10–15 % when 100 % Ar is used, with higher values occasionally occurring under certain conditions. This decrease in stability may, in part, be due to the "deposition" of ablated particles next to the ablated line when a higher percentage of Ar is used. These deposits can be ablated during subsequent ablation passes, leading to signal "outliers" and fluctuations in subsequent line scan data. It should also be considered that the standard ablation cell is optimized for helium as the primary carrier gas, so the different physical properties of argon result in lower particle transport efficiency.

Table 2
Instrumental parameters used at the NIC LA-ICP-MS system.

LA (Analyte G2, ARIS)	
Wavelength (nm)	193
Laser fluence (J cm-2)	3.5
Repetition rate (Hz)	250
Scanning mode	Line scanning
Dosage (shots per pixel)	20
Washout time (ms)	ca. 40
Beam size (μm)	10, 20, 35
Mask shape	Square
He carrier flow rate (L min-1) cup|cell	0.3|0.3
ICP-MS (Agilent 7900x)	
Rf power (W)	1500
Plasma gas flow rate (L min-1)	15
Auxiliary gas flow rate (L min-1)	0.9
Ar makeup flow rate (L min-1)	0.8
Data acquisition	Time-resolved
Dwell time (ms)	6.5
Acquisition time (ms)	40
Nuclides measured	^{7}Li, ^{89}Y, ^{232}Th, ^{238}U

3.2. Mapping performance in Ar conditions on murrina glass

We used a freshly polished surface of the murrina glass to assess the mapping performance under 100 % He and Ar conditions, respectively and using both the cup and tube cell configurations with the AWI cryo-LA-ICP-TOFMS. Fig. 5 shows representative examples of the obtained maps. We take the maps obtained under He conditions as a reference for typical map quality, showing clearly defined features among different elemental channels. In contrast, using the cup cell configuration, we find some elemental maps being strongly influenced by a high degree of noise and spurious groups of high intensity pixels. Using the tube cell configuration, these noise-components disappear and the map quality improves further if mapped at 250 Hz (shown in Fig. 5).

Notably, all maps obtained in Ar show significantly lower intensities as compared to He. Although the difference varies slightly among elements, intensities are typically close to a factor of 2 higher in He vs Ar. The large amount of noise in the signal under cup cell configuration with Ar are also present in single pulses recorded on NIST SRM 612. Typical SPR values remained around 100 ms but show a very noisy peak shape. Using the tube cell configuration, on the other hand, it is possible to obtain clearly defined peaks within 10–20 ms (FW0.1M). For this purpose, both gas flows and distance to sample are tuned. Gas flows are generally lower than for pure He conditions, while the distance between the sample surface and aerosol collection port remains similar (400–600 μm). Fig. 6 shows an exemplary comparison of single pulse peak shapes obtained under pure He and Ar conditions, respectively.

3.3. Mapping in Ar versus He conditions on ice cores

Both directions were tested: Mapping in He first, then switching to Ar and vice versa, without a discernible visual difference in the results. After switching the gas lines and reprogramming the mass flow controllers for Ar or He respectively, the cell was evacuated 20 times, following the standard procedure that is followed also after any sample exchange. This ensures a complete removal of the old gas and flushing of the cell with the new gas. The cell conditions (gas flows, sample distance) are adjusted to achieve SPR like in Fig. 6 but other changes to the instrument are avoided. Fig. 7 shows example maps obtained in He and Ar at the same location on the ice surface. The same features are present in both sets of maps: the grain boundary network and sporadic groups of high intensity pixels in the grain interiors, which are likely caused by insoluble dust particles [15]. Notably, maps using Ar as a carrier gas

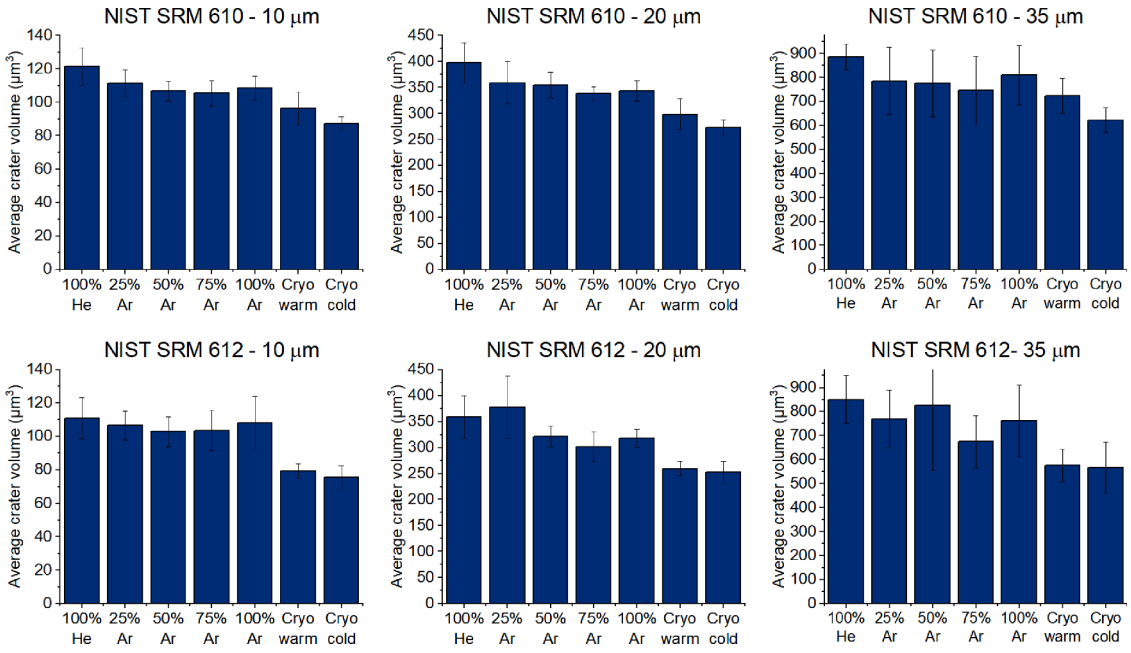

Fig. 2. Crater volume on NIST SRM 610 and 612 with different spot sizes measured for He and Ar as well as He/Ar mixes (top row, a). The bottom row (b) shows two examples of the crater morphology of 10 µm square spot under 100 % He (left) and Ar (right), respectively.

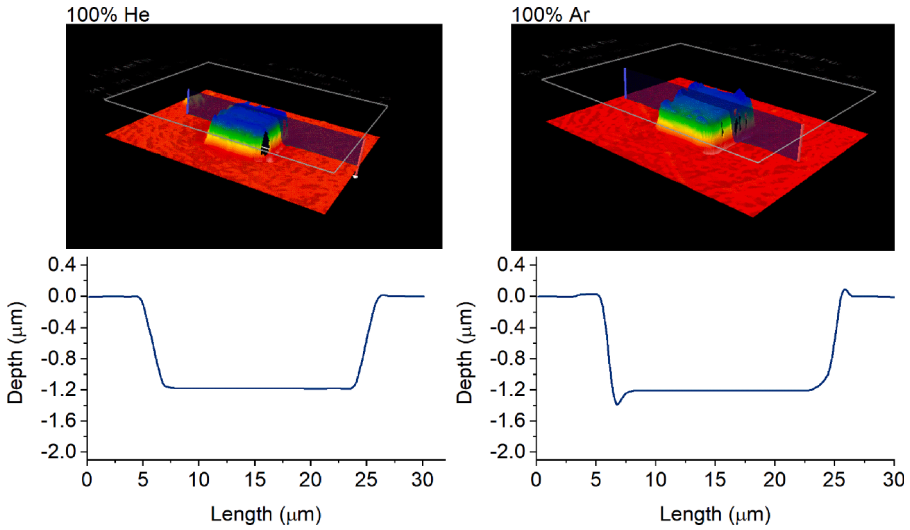

Fig. 3. Two examples of the crater morphology of 10 µm square spot under 100 % He (left) and Ar (right), respectively, obtained on NIST SRM 612.

generally feature higher intensities as compared to He. This effect occurs regardless of the order of map acquisition (He first, Ar second, or vice versa).

Fig. 8 shows the intensity ratio between Ar and He maps for the elemental spectrum recorded and divided by image features after segmenting the grain boundaries in the maps analogue to previous studies [15]: Intensity ratios at the grain boundaries only (GB) and in the grain interiors (INT). On average, intensities are about 1.5 times higher in Ar than in He. The deep interglacial ice sample constitutes an extreme case in this regard, for which only noise was recorded under He conditions. After switching to Ar carrier gas, the expected signals from grain boundaries could be detected clearly (Fig. 9).

In order to further investigate the relative increase in signal in Ar over He for ice, we calculated the following: The maps typically feature a bimodal distribution with one large mode corresponding to the dark low-intensity pixels in the maps, and a smaller mode corresponding to the high intensity pixels constituting the "signal" (primarily at the grain boundaries). We applied a manual threshold to carefully separate the two modes and to subsequently calculate their means and the ratio of the means. The latter serves as an estimate of the signal to noise in the maps. To quantify the relative increase in signal to noise for Ar, the signal to noise estimates of Ar was divided by the one obtained for He. The corresponding data is plotted in yellow in Fig. 8.

4. Discussion

4.1. Mapping in Ar conditions

Many previous studies showed that using He instead of Ar as a carrier gas enhances signals for 193 nm lasers, which was attributed to a decrease of re-deposited material, improved transportation efficiency of smaller particles and agglomerates, coupled with an increased ionization efficiency in the ICP-MS [e.g. 23]. The smaller particle size is explained by the higher thermal conductivity and lower viscosity of He

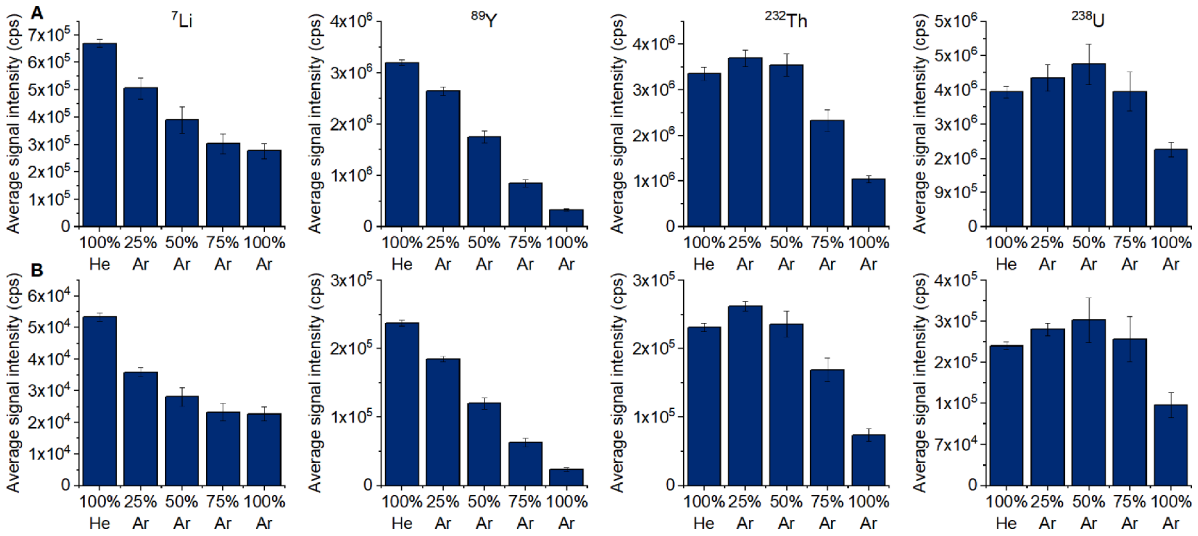

Fig. 4. Comparison of signal intensity on NIST 610 and 612, in row A and B, respectively. Shown from left to right in each panel are 100 % He, mixes with 25, 50 and 75 % Ar, and 100 % Ar.

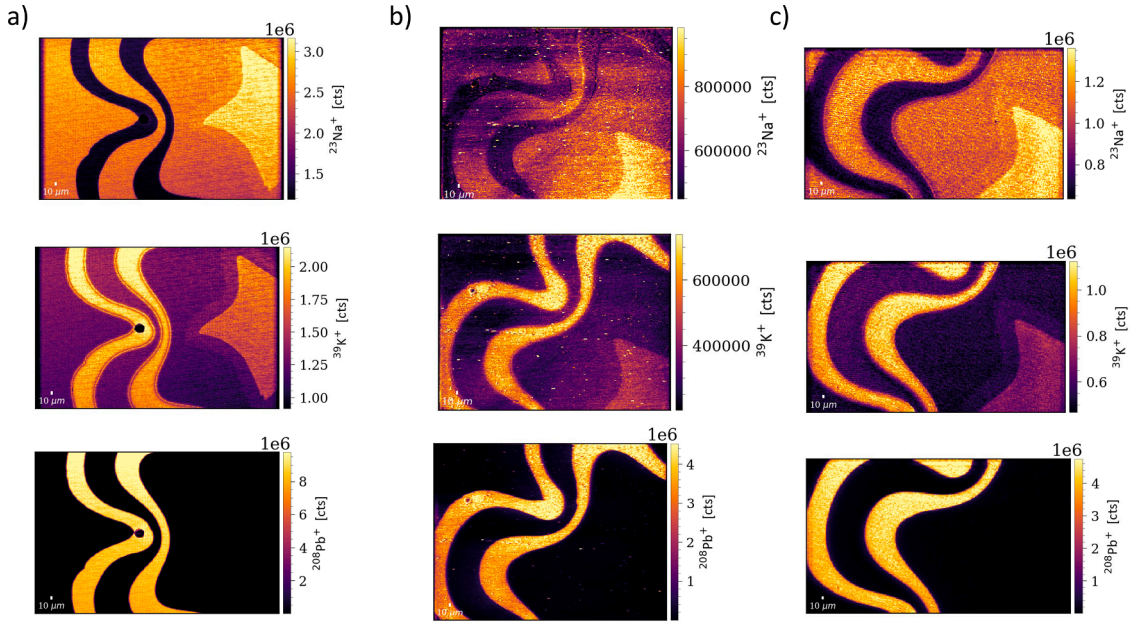

Fig. 5. Comparison of elemental maps obtained in cup cell configuration in He (2 × 3 mm, a) and Ar (2 × 2.6 mm, b) at 500 Hz, and in the tube cell configuration using Ar as carrier gas (1.5 × 2.5 mm, c) at 250 Hz. Note the scale on all maps is in 10^6 counts except for ^{23}Na and ^{39}K.

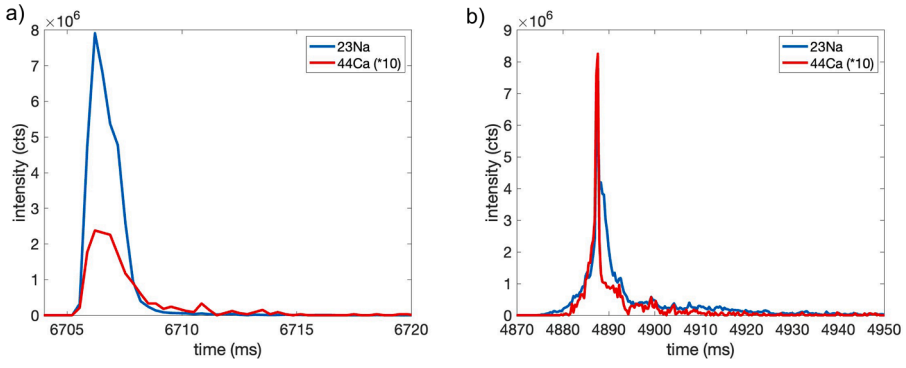

Fig. 6. Representative single pulse response peaks obtained on NIST SRM 612 with a 10µm spot using the tube cell configuration in He (a) and Ar (b) carrier gas conditions. Note that the ^{44}Ca intensity is scaled by a factor of 10 for better visibility.

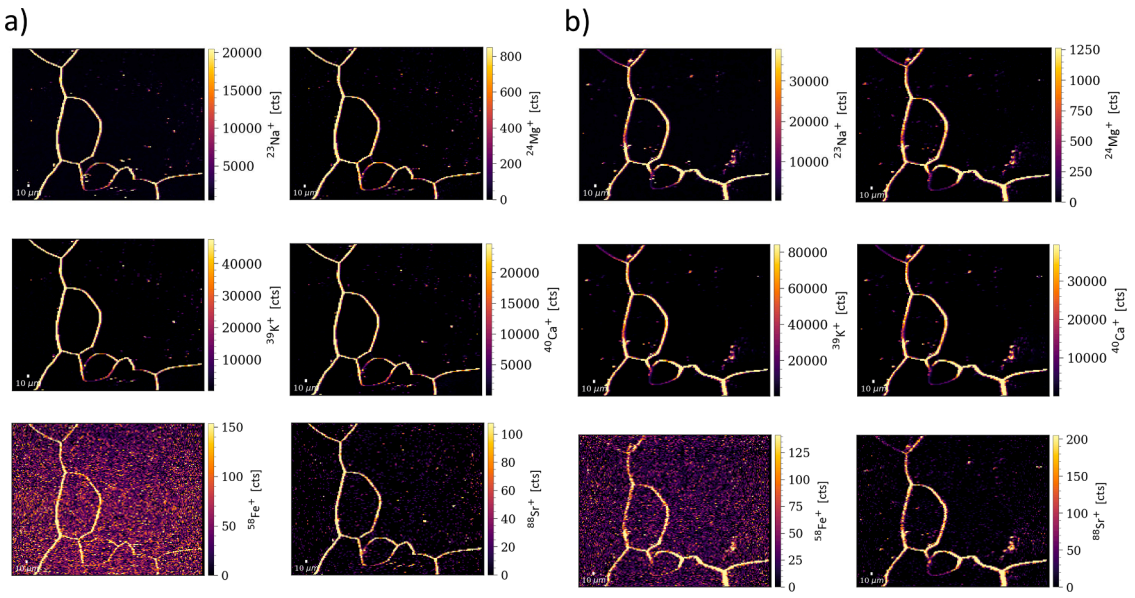

Fig. 7. Ice core impurity maps on Antarctic ice from a glacial period (EDC1819-3). The same area was ablated at 250 Hz (see text) in He (a) and Ar (b). Map size is 1.5 × 1.9 mm, the corresponding mosaic is shown in Fig. 1 b). Note the differences in intensities between He (a) and Ar (b) (in cts).

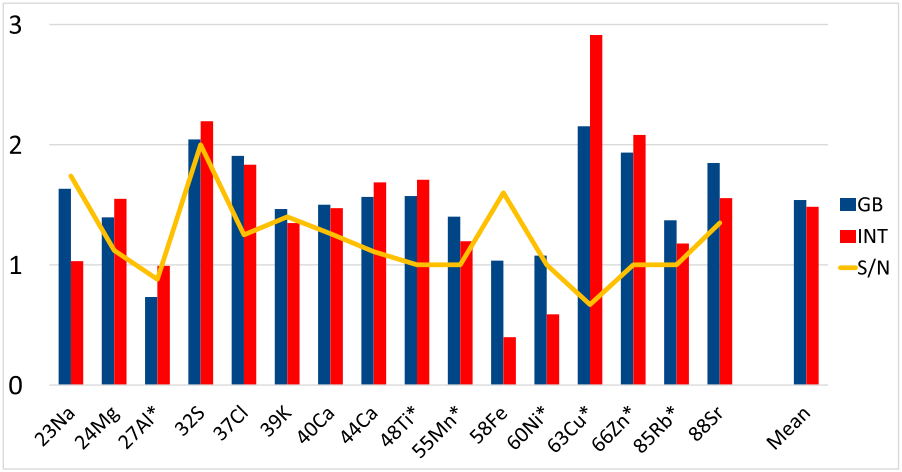

Fig. 8. Intensity ratio for the map shown in Fig. 7, dividing Ar/He carrier gas maps for pixels belonging to grain boundaries (GB) and grain interiors (INT). The acquired mass range was from m/z=23 up to m/z=90. Channels with only weak signals are marked with a star (*). Channels with only noise have been removed. The yellow line shows the relative increase in signal-to-noise in Ar (see text). (For interpretation of the references to colour in this figure legend, the reader is referred to the web version of this article.)

compared with Ar, resulting in a faster spread of thermal energy and less condensational growth [21]. Our results confirm this view by showing that the crater morphology shows no substantial differences between ablation in He and Ar, indicating that the amount of ablated material remains largely unchanged. The cooling by the cryogenic holder realizes a roughly 40 °C temperature difference at the sample surface with respect to uncooled conditions, which does not appear to be of significance to reduce any thermal effects such as minimizing condensational growth. This is consistent with a recent study observing a distinct suppressing of thermal effects by cryogenic temperatures on sulfide matrices but not on silicates (NIST glass) [29].

The fact that aerosol collection using a cup cell results in long and unstable SPR in Ar conditions also confirms the importance of efficient aerosol collection and transport. The dispersed spots of high intensity pixels in the murrina maps could indicate that ejecta are re-deposited on the sample surface, albeit to a variable degree depending on the element. Notably, in Ar conditions we also observed deposited aerosol around the end of the peek tubing delivering the aerosol to the torch injector. Using the tube cell in Ar condition offers a more efficient collection and transport of the generated aerosol, demonstrated by the more stable SPR in the range of a few 10 ms. Another study demonstrated that the loss in sensitivity in Ar conditions can be mitigated by collecting the aerosol under a high gas velocity regime [22]. We interpret the difference between the cup and tube cell as a similar effect, due to the laminar gas flow within the tube cell [30]. Based on the achieved SPR, artifact-free maps could be obtained at repetition rates up to 500 Hz, demonstrating that state-of-the-art mapping is possible in Ar using a commercial system that has been designed for He as a carrier gas. This already indicates that the performance in Ar conditions might be substantially increased, e.g. by a device for aerosol transfer specifically engineered for Ar. Such a device might also help to mitigate the lower sensitivity in Ar seen in the murrina maps, which is consistent with the previously demonstrated sensitivity gain of He over Ar.

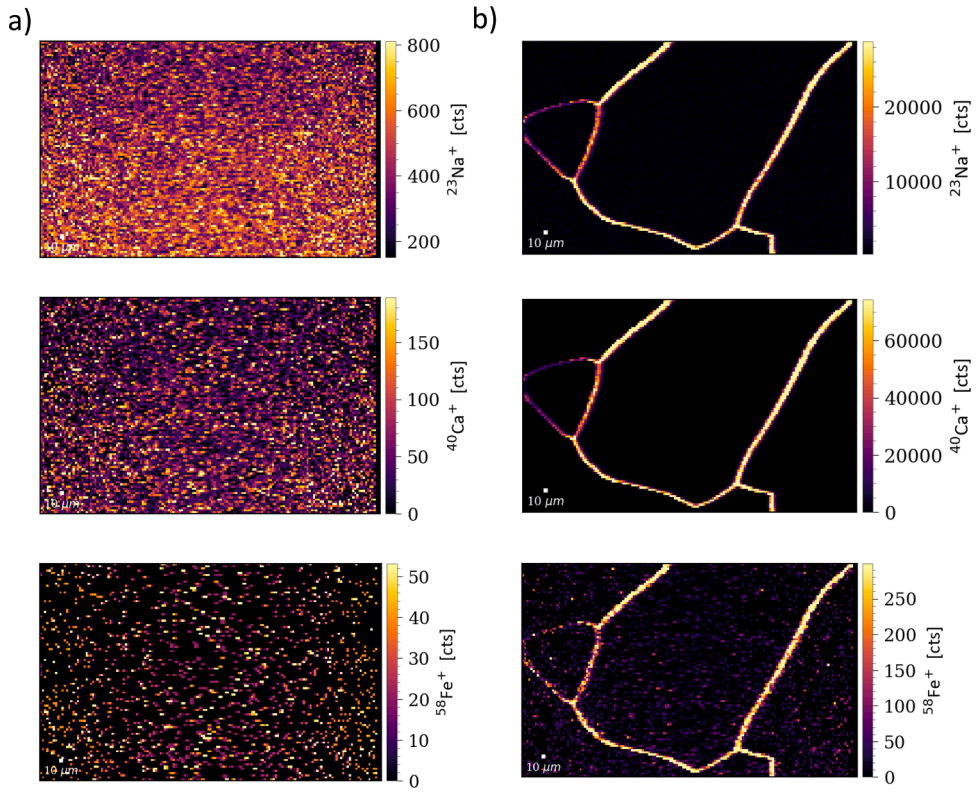

Fig. 9. Ice core impurity maps on Antarctic ice from an interglacial period. The same area was ablated two times at 500 Hz (see text), first in He (a) and then in Ar (b). Map size is 1 × 1.6 mm, the corresponding mosaic is shown in Fig. 1 c).

4.2. Potential merit of Ar as a carrier gas for ice core impurity mapping

Using Ar as a carrier gas, mapping on ice is possible without any visible degradation in map quality, even at 500 Hz (Fig. 9). From an economical point of view this makes Ar a cost-effective alternative to He, especially when used in large volume cryocells, e.g. as envisaged for the upcoming analysis of the "Oldest Ice Core". From an analytical point of view, the observed increase in sensitivity under Ar conditions is intriguing especially for the analysis of Antarctic interglacial ice with very low impurity concentrations. Compared to the sensitivity decrease observed on the murrina glass with the same setup and identical measurement technique, it is plausible to explain the sensitivity enhancement in Ar with the water-based matrix. Several studies have shown that the addition of a small amount of water into the ICP will lead to increased sensitivity due to a more complete vaporization through a more efficient energy transfer to the aerosol, although the magnitude of the effect may depend on the specific ICP-MS instrument [22,23,31]. Ablating ice would inherently lead to such a minor flux of water vapor with the aerosol, which was already suspected by Reinhardt et al. [18] and has recently been confirmed also experimentally [32]. However, the extreme example of Fig. 9, showing an increase in intensities by 1–2 orders of magnitude in Ar versus He suggests that a different additional effect is likely involved. Pure ice is highly transparent within the UV range and at 193 nm in particular [33]. Recent empirical evidence on artificial ice samples showed that the impurity load can enhance the ablation response to 193 nm nanosecond lasers, and that low-level impurity ice is more resilient to ablation at high fluence [16]. Using Ar, a different thermal regime around the ablation zone may help to increase the coupling efficiency of the laser with the ice, hence making a noticeable difference in the ablation behavior under ultra-clean conditions of deep Antarctic interglacial ice samples. Apart from optical estimates of the crater depth imprinted by several hundred shots [9], no direct measurements of the ablated crater volumes in ice have been performed, not least due to the complexity of using cryogenic holders and the influence of sublimation under dry He or Ar atmospheres.

The difference in ablation characteristics in He versus Ar would also need to be taken into account when attempting a calibration with artificial ice standards, which would need to be investigated for the same effect to provide "matrix-matched" conditions. In any case, the example of Fig. 9 clearly demonstrates the potential of Ar for retrieving signals from ultra-clean ice samples with a 193 nm laser. Such qualitative maps are already sufficient for studying the 2D impurity distribution, studying relative variability of climate signals and assessing layer signal preservation. On the other hand, taken together with recent evidence of isotopic fractionation processes during ablation with a 193 nm nanosecond laser on ice [32], this finding stresses the need for further research into ice-laser interaction, including assessing the potential merits of femtosecond lasers.

5. Conclusions

LA-ICP-MS mapping has delivered important new insight into the micro-chemistry of ice cores, which comes at a crucial moment in the field of ice core science, currently targeting the oldest layers in Antarctica. Further refinements of the technique may further extend its potential, however. Here we explored the use of Ar as a more economical carrier gas alternative to He, especially within the framework of developing large cryocell technology. Based on previous studies demonstrating the analytical benefits of enhancing sensitivity by introducing "moist Ar", investigating this effect on a water-based matrix has been an obvious additional component in this study. We have confirmed that while crater morphology remains almost unchanged in Ar versus He, aerosol transfer plays a critical role. The use of a tube cell has shown to deliver SPR of a few ten milliseconds, which was not possible with the use of a cup cell. Based on the achieved SPR, artifact-free maps could be obtained at up to 500 Hz, demonstrating that state-of-the-art mapping is possible in Ar using a commercial system that has been designed around He as a carrier gas. This already indicates that the performance in Ar

conditions might be substantially increased, e.g. by a device for aerosol transfer specifically engineered for Ar. Although we find lower sensitivities for the maps obtained in Ar on the murrina glass, users analyzing similar impurity-rich matrices may be able to manage this sensitivity decrease and value the decrease in consumable costs by using Ar over He. The latter aspect will become especially relevant for using large sample cell technology with high gas consumption. In contrast to the murrina glass, on ice we find clear evidence for an increase in sensitivity, which can be crucial in analyzing low impurity Antarctic interglacial ice, but also raises further question regarding the ice-laser interaction.

Data availability

The underlying data used for creating the chemical maps in the study are available at zenodo.org via https://doi.org/10.5281/zenodo.15068538 with license Creative Commons Attribution 4.0 International.

CRediT authorship contribution statement

Pascal Bohleber: Writing – original draft, Visualization, Methodology, Investigation, Funding acquisition, Formal analysis, Conceptualization. **Kristina Mervič:** Writing – original draft, Visualization, Methodology, Investigation, Funding acquisition, Formal analysis. **Remi Dallmayr:** Writing – original draft, Methodology, Investigation. **Ciprian Stremtan:** Writing – original draft, Methodology, Investigation, Conceptualization. **Martin Šala:** Writing – original draft, Methodology, Investigation, Funding acquisition, Conceptualization.

Declaration of competing interest

The authors declare that they have no known competing financial interests or personal relationships that could have appeared to influence the work reported in this paper.

Acknowledgements

We are grateful to Carlo Barbante and his group (Ca'Foscari University of Venice, Italy) for lending us the cryogenic sample holder and related equipment for the experiments performed at NIC in Ljubljana. Co-funded by the European Union (ERC, AiCE, 101088125). Views and opinions expressed are however those of the authors only and do not necessarily reflect those of the European Union or the European Research Council. Neither the European Union nor the granting authority can be held responsible for them. The authors acknowledge the financial support from the Slovenian Research Agency ARRS research core fundings no. P1-0034 and no. P2-0152.

References

[1] H. Fischer, T. Blunier, R. Mulvaney, Ice Cores: Archive of the Climate System, Springer, 2021.
[2] M. Legrand, P. Mayewski, Glaciochemistry of polar ice cores: a review, Rev. Geophys. 35 (3) (1997) 219–243, https://doi.org/10.1029/96rg03527.
[3] G. Baccolo, B. Delmonte, E. Di Stefano, G. Cibin, I. Crotti, M. Frezzotti, et al., Deep ice as a geochemical reactor: insights from iron speciation and mineralogy of dust in the Talos Dome ice core (East Antarctica), The Cryosphere 15 (10) (2021) 4807–4822, https://doi.org/10.5194/tc-15-4807-2021.
[4] F. Lambert, B. Delmonte, J.R. Petit, M. Bigler, P.R. Kaufmann, M.A. Hutterli, et al., Dust - climate couplings over the past 800,000 years from the EPICA Dome C ice core, Nature 452 (7187) (2008) 616–619, https://doi.org/10.1038/nature06763.
[5] R. Traversi, S. Becagli, E. Castellano, F. Marino, F. Rugi, M. Severi, et al., Sulfate spikes in the deep layers of EPICA-Dome C ice core: evidence of glaciological artifacts, Environ. Sci. Technol. 43 (23) (2009) 8737–8743, https://doi.org/10.1021/es901426y.
[6] E.J. Brook, E. Wolff, D. Dahl-Jensen, H. Fischer, E.J. Steig, The future of ice coring: international partnerships in ice core sciences (IPICS), PAGES News 14 (1) (2006) 6–10, https://doi.org/10.22498/pages.14.1.6.
[7] H. Fischer, J. Severinghaus, E. Brook, E. Wolff, M. Albert, O. Alemany, et al., Where to find 1.5 million yr old ice for the IPICS "oldest-ice" ice core, Clim. Past 9 (6) (2013) 2489–2505, https://doi.org/10.5194/cp-9-2489-2013.
[8] N. Stoll, P. Bohleber, R. Dallmayr, F. Wilhelms, C. Barbante, I. Weikusat, The new frontier of microstructural impurity research in polar ice, Ann. Glaciol. 64 (91) (2023) 63–66.
[9] W. Müller, J.M.G. Shelley, S.O. Rasmussen, Direct chemical analysis of frozen ice cores by UV-laser ablation ICPMS, J. Anal. At. Spectrom. 26 (12) (2011) 2391–2395, https://doi.org/10.1039/c1ja10242g.
[10] S.B. Sneed, P.A. Mayewski, W.G. Sayre, M.J. Handley, A.V. Kurbatov, K.C. Taylor, et al., New LA-ICP-MS cryocell and calibration technique for sub-millimeter analysis of ice cores, J. Glaciol. 61 (226) (2015) 233–242, https://doi.org/10.3189/2015jog14j139.
[11] D. Della Lunga, W. Müller, S.O. Rasmussen, A. Svensson, Location of cation impurities in NGRIP deep ice revealed by cryo-cell UV-laser-ablation ICPMS, J. Glaciol. 60 (223) (2014) 970–988, https://doi.org/10.3189/2014JoG13J199.
[12] D. Della Lunga, W. Müller, S.O. Rasmussen, A. Svensson, P. Vallelonga, Calibrated cryo-cell UV-LA-ICPMS elemental concentrations from the NGRIP ice core reveal abrupt, sub-annual variability in dust across the GI-21.2 interstadial period, The Cryosphere 11 (3) (2017) 1297–1309, https://doi.org/10.5194/tc-11-1297-2017.
[13] P. Bohleber, M. Roman, M. Šala, C. Barbante, Imaging the impurity distribution in glacier ice cores with LA-ICP-MS, J. Anal. At. Spectrom. 35 (10) (2020) 2204–2212.
[14] P. Bohleber, M. Roman, M. Šala, B. Delmonte, B. Stenni, C. Barbante, Two-dimensional impurity imaging in deep antarctic ice cores: snapshots of three climatic periods and implications for high-resolution signal interpretation, The Cryosphere 15 (7) (2021) 3523–3538, https://doi.org/10.5194/tc-15-3523-2021.
[15] P. Bohleber, N. Stoll, M. Rittner, M. Roman, I. Weikusat, C. Barbante, Geochemical characterization of insoluble particle clusters in ice cores using two-dimensional impurity imaging, Geochem. Geophys. Geosyst. 24 (2) (2023) e2022GC010595.
[16] P. Bohleber, P. Larkman, N. Stoll, D. Clases, R. Gonzalez de Vega, M. Šala, et al., Quantitative insights on impurities in ice cores at the micro-scale from calibrated LA-ICP-MS imaging, Geochem. Geophys. Geosyst. 25 (4) (2024) e2023GC011425.
[17] N.E. Spaulding, S.B. Sneed, M.J. Handley, P. Bohleber, A.V. Kurbatov, N.J. Pearce, et al., A new multielement method for LA-ICPMS data acquisition from glacier ice cores, Environ. Sci. Technol. 51 (22) (2017) 13282–13287, https://doi.org/10.1021/acs.est.7b03950.
[18] H. Reinhardt, M. Kriews, H. Miller, O. Schrems, C. Lüdeke, E. Hoffmann, J. Skole, Laser ablation inductively coupled plasma mass spectrometry: a new tool for trace element analysis in ice cores, Fresenius J. Anal. Chem. 370 (5) (2001) 629–636, https://doi.org/10.1007/s002160100853.
[19] D. Käser, R. Kägi, B. Hattendorf, D. Gunther, Fundamental studies of laser ablation ICPMS using a nitrogen plasma source and helium, argon and nitrogen as carrier gas, J. Anal. At. Spectrom. (2024).
[20] J. Koch, M. Wälle, S. Schlamp, T. Rösgen, D. Günther, Expansion phenomena of aerosols generated by laser ablation under helium and argon atmosphere, Spectrochim. Acta, Part B 63 (1) (2008) 37–41.
[21] I. Horn, D. Günther, The influence of ablation carrier gasses ar, he and ne on the particle size distribution and transport efficiencies of laser ablation-induced aerosols: implications for LA-ICP-MS, Appl. Surf. Sci. 207 (1–4) (2003) 144–157.
[22] T. Luo, Z. Hu, W. Zhang, D. Günther, Y. Liu, K. Zong, S. Hu, Reassessment of the influence of carrier gases he and ar on signal intensities in 193 nm excimer LA-ICP-MS analysis, J. Anal. At. Spectrom. 33 (10) (2018) 1655–1663.
[23] D. Günther, C.A. Heinrich, Enhanced sensitivity in laser ablation-ICP mass spectrometry using helium-argon mixtures as aerosol carrier, J. Anal. At. Spectrom. 14 (9) (1999) 1363–1368.
[24] T. Van Acker, S.J. Van Malderen, T. Van Helden, C. Stremtan, M. Šala, J.T. van Elteren, F. Vanhaecke, Analytical figures of merit of a low-dispersion aerosol transport system for high-throughput LA-ICP-MS analysis, J. Anal. At. Spectrom. 36 (6) (2021) 1201–1209.
[25] S.J. Van Malderen, T. Van Acker, F. Vanhaecke, Sub-micrometer nanosecond LA-ICP-MS imaging at pixel acquisition rates above 250 Hz via a low-dispersion setup, Anal. Chem. 92 (8) (2020) 5756–5764.
[26] m. EPICA community, Eight glacial cycles from an antarctic ice core, Nature 429 (2004) 623–628, https://doi.org/10.1038/nature02599.
[27] J.T. van Elteren, V.S. Šelih, M. Šala, Insights into the selection of 2D LA-ICP-MS (multi) elemental mapping conditions, J. Anal. At. Spectrom. 34 (9) (2019) 1919–1931.
[28] K. Mervič, J.T. van Elteren, M. Bele, M. Šala, Utilizing ablation volume for calibration in LA-ICP-MS mapping to address variations in ablation rates within and between matrices, Talanta 269 (2024) 125379, https://doi.org/10.1016/j.talanta.2023.125379.
[29] H. Li, F. Li, W. Guo, L. Jin, S. Hu, Simple strategy to suppress the thermal effect for multi-element analysis in sulfide minerals by LA-ICP-MS with a cryogenic ablation cell, J. Anal. At. Spectrom. 39 (6) (2024) 1493–1502.
[30] S.J. Van Malderen, A.J. Managh, B.L. Sharp, F. Vanhaecke, Recent developments in the design of rapid response cells for laser ablation-inductively coupled plasma-mass spectrometry and their impact on bioimaging applications, J. Anal. At. Spectrom. 31 (2) (2016) 423–439.
[31] L. Flamigni, J. Koch, D. Günther, The effect of carrier gas humidity on the vaporization of laser-produced aerosols in inductively coupled plasmas, J. Anal. At. Spectrom. 29 (2) (2014) 280–286.
[32] E. Malegiannaki, P. Bohleber, D. Zannoni, C. Stremtan, A. Petteni, B. Stenni, V. Gkinis, Towards high-resolution water isotope analysis in ice cores using laser ablation-cavity ring-down spectroscopy, Analyst (2024).
[33] S.G. Warren, R.E. Brandt, Optical constants of ice from the ultraviolet to the microwave: a revised compilation, J. Geophys. Res. Atmos. 113 (D14) (2008).